JMEPEG (2008) 17:535–542
DOI: 10.1007/s11665-007-9174-4

1059-9495/$19.00

Investigations on Heat Treatment of a High-Speed Steel Roll

Hanguang Fu, Yinhu Qu, Jiandong Xing, Xiaohui Zhi, Zhiqiang Jiang, Mingwei Li, and Yi Zhang

(Submitted March 16, 2007; in revised form September 21, 2007)

High-carbon high-speed steels (HSS) are very abrasion-resistant materials primarily due to their high hardness MC-type carbide and high hardness martensitic matrix. The effects of quenching and tempering treatment on the microstructure, mechanical properties, and abrasion resistance of centrifugal casting high-carbon HSS roll were studied. Different microstructures and mechanical properties were obtained after the quenching and tempering temperatures of HSS roll were changed. With air-cooling and sodium silicate solution cooling, when the austenitizing temperature reaches 1273 K, the metallic matrix all transforms into the martensite. Afterwards, the eutectic carbides dissolve into the metallic matrix and their continuous network distribution changes into the broken network. The second hardening temperature of high-carbon HSS roll is around 793 K. No significant changes in tensile strength and elongation percentage are observed unless the tempering temperature is beyond 753 K. The tensile strength increases obviously and the elongation percentage decreases slightly beyond 753 K. However, the tensile strength decreases and the elongation percentage increases when the tempering temperature exceeds 813 K. When the tempering temperature excels 773 K, the impact toughness has a slight decrease. Tempering at 793-813 K, high-carbon HSS roll presents excellent abrasion resistance.

Keywords abrasion resistance, high-carbon HSS roll, mechanical property, quenching temperature, tempering temperature

1. Introduction

The development of the steel rolling industries puts forward higher requirement on the mechanical properties and abrasion resistance of the rolls (Ref 1, 2). The application of high-carbon high-speed steel (HSS) replacing high-chromium cast iron is one of the recent developments in the manufacture of rolls employed in the steel production (Ref 3-6). Currently, many methods such as centrifugal casting (Ref 7, 8), electric slag remelting (Ref 9), continuous pouring process for cladding (CPC) (Ref 10), hot isostatic pressing (Ref 11), and spray forming (Ref 12, 13), etc., have been used to fabricate the compound high-carbon HSS work roll. Thereinto, the centrifugal process, which is commonly used for its high productivity and cost advantage, has extensively been applied to the production of HSS roll (Ref 7, 8, 14-16).

Hanguang Fu, Research Institute of Advance Materials Processing Technology, School of Materials Science and Engineering, Beijing University of Technology, Beijing 100022, P.R. China; **Hanguang Fu, Jiandong Xing, Xiaohui Zhi,** and **Zhiqiang Jiang**, State Key Laboratory of Mechanical Behavior of Materials, School of Materials Science and Engineering, Xi'an Jiaotong University, Xi'an, Shaanxi Province 710049, P.R. China; **Yinhu Qu**, School of Electromechanical Engineering, Xi'an Polytechnic University, Xi'an, Shaanxi Province 710048, P.R. China; and **Mingwei Li** and **Yi Zhang**, Chongqing Qhuanshen Harbor Machinery Manufacture Co. Ltd., Chongqing 400045, P.R. China. Contact e-mail: fhg64@263.net.

Many researches discovered that the increased vanadium concentration and high-hardness MC carbide in high-carbon HSS promoted excellent wear resistance and a service life that is many times longer than that of the cast iron roll (Ref 17, 18). The excellent wear resistance of high-carbon HSS is primarily caused by the favorable morphology and resisting crush capacity of MC type carbide, and high-hardness matrix as well (Ref 17). The structures and properties of high-carbon HSS roll depend on a heat treatment process (Ref 19-21). Zhou et al. (Ref 19) puts forward that the peak hardness temperature of high-carbon HSS is about 150-250 K lower than the conventional high-speed steel, and it decreases with the increase of carbon concentration and increases with the increase of vanadium concentration. Then Zhao et al. (20) further discovers that the second hardening temperature of high-carbon HSS is about 823 K and one tempering treatment is enough to meet the requirement of roll. Moreover, the adoption of laser transformation hardening can improve the surface hardness of high-carbon HSS roll apparently. When the highest hardness value reaches 68.5 HRC, the spheroidal carbides distribute dispersively over the matrix, and the wear resistance of HSS rolls increases obviously (Ref 22). However, the effects of tempering temperature on the tensile strength, the impact toughness, and the abrasion resistance of high-carbon HSS roll fabricated by centrifugal casting have no particular study. The heat treatment process needs to be improved in order to increase the abrasion resistance of high-carbon HSS roll.

In this article, we attempt to investigate the effects of austenitizing temperature, quenchant, and tempering temperature on the microstructures, mechanical properties, and wear resistance of centrifugal casting high-carbon HSS roll. The optimum heat treatment process has been determined, which can be used to instruct the heat treatment of high-carbon HSS roll.

2. Experimental

2.1 Smelting and Casting of High-Carbon HSS Roll

The alloy used in this study was prepared in a 350 kg medium frequency furnace by air melting using pig iron and carbon steel as the base metal with the addition of ferrovanadium, ferromolybdenum, ferrotungsten, ferrochromium, ferroniobium, pure cobalt, and nickel as the alloy elements. Pure aluminum was added for deoxidization and the rolls were fabricated by a horizontal centrifugal casting apparatus. The melt was charged into a high-speed revolving mold to form a shell part at a temperature of 1753 K. The size of HSS roll billet was Ø350 mm × 800 mm; the thickness of the shell of HSS roll billet was 90 mm. HSS roll billet was machined into the finished roll. The shape and dimensions of finished HSS roll are shown in Fig. 1. The units of the dimensions of the finished roll in Fig. 1 are in millimeter. The chemical compositions of HSS roll are shown in Table 1.

2.2 Heat Treatment

The specimens were heat treated by austenitizing at 1173-1473 K for 60 min under a controlled atmosphere and cooled in the sodium silicate solution and in the air, respectively, and then tempered at 473-873 K for 120 min in the air. The density of sodium silicate solution was 1.18 g/cm^3. The cooling rates of sodium silicate solution and air were 28.4 and 7.8 °C/s, respectively.

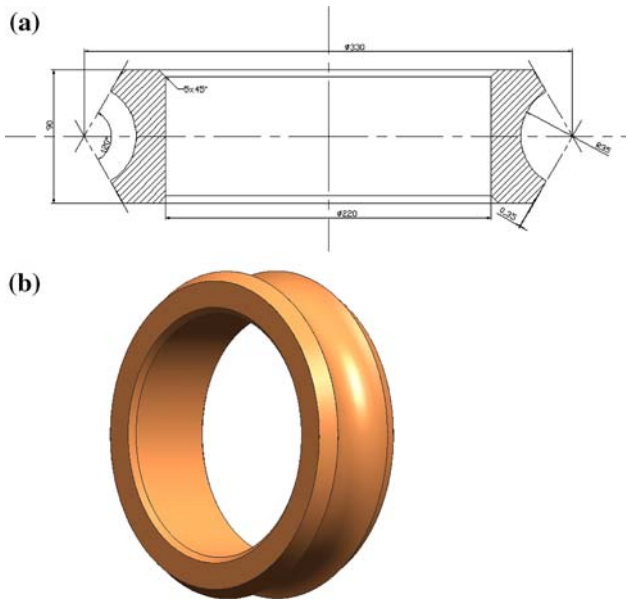

Fig. 1 The shape and dimensions of finished HSS roll: (a) dimension drawing; and (b) outside drawing

Table 1 Chemical compositions of HSS roll (wt.%)

Elements	C	V	Mo	W	Cr	Nb	Co
Composition	1.88	4.89	5.93	2.03	6.05	4.08	5.02
Elements	**Ni**	**Si**	**Mn**	**S**	**P**	**Al**	**Fe**
Composition	0.99	1.23	0.86	0.02	0.03	0.06	Bal.

2.3 Mechanical Property Measurement

The hardness measurement of the samples was done using an HR-150A type hardness tester. At least five indentations were made on each sample under each experimental condition to check reproducibility of the hardness data. The tensile tests were performed on a universal material testing machine according to ASTM standard E-8 (Ref 23), the dimensions of specimens were Ø10 mm × 130 mm. Three identical specimens were tested, and the ultimate tensile strength and percentage of elongation were determined from the load-displacement diagrams. Charpy unnotched impact tests were performed at room temperature using a 300 J capacity machine, the dimensions of specimens were 10 mm × 10 mm × 55 mm. The average values from three test specimens were reported here.

The retained austenite content of the matrix was determined using X-ray diffraction (Ref 24-26). A special sample holder, which continuously tilted and rotated the sample, was used to eliminate orientation effects (Ref 27). The results are given as the proportion of austenite in the matrix, based on a direct comparison of the intensity of the γ_{220}, γ_{311}, α_{200}, and α_{211} diffraction peaks according to Eq 1 (Ref 28, 29)

$$V_\gamma = \frac{1 - V_C}{1 + k\frac{I_{\alpha(hkl)i}}{I_{\gamma(hkl)j}}} \quad \text{(Eq 1)}$$

where V_γ and V_C are the volume fraction of the retained austenite and carbide in the high-carbon HSS, respectively, thereinto, the carbide volume fraction is obtained by image analysis using Leica digital images analyzer after deep-etching the samples in a solution of ferric chloride. $I_{\alpha(hkl)i}$ and $I_{\gamma(hkl)j}$ are the intensity of the certain crystal planes of martensite and austenite, respectively. K, as shown in Table 2 (Ref 30), is the scale factor between $I_{\alpha(hkl)i}$ and $I_{\gamma(hkl)j}$.

2.4 Abrasion Resistance Measurement

The sliding wear tests were conducted using a high-temperature wear test machine, which was improved through a ML-10 type pin abrasion tester (Ref 31, 32). This wear test procedure had been reported previously when characterizing the tool steel at high temperature (Ref 33, 34). Figure 2 was the schematic diagram of wear test device. It was made up of the mechanical drive part, the heating part, and the controlling temperature part. Pins of 6.0 mm diameter and 25 mm height were worn for 15 min against a 60 mm diameter counterface disc made of hardened M2 steel, at a sliding speed of 0.1 m/s. All the materials were tested under the same conditions. The wear tests were carried out at 773 and 923 K in air, with a relative humidity of ~60%, and a normal load of 20 and 80 N, respectively. After being abraded, the pins were ultrasonically cleaned in warm soapy water and then in ethanol for several minutes and dried in hot air. The mass losses of the specimens

Table 2 Values of K between $I_{\alpha(hkl)i}$ and $I_{\gamma(hkl)j}$

Plane of austenite	Plane of martensite	K
(220)	(211)	0.65
(311)	(200)	0.87

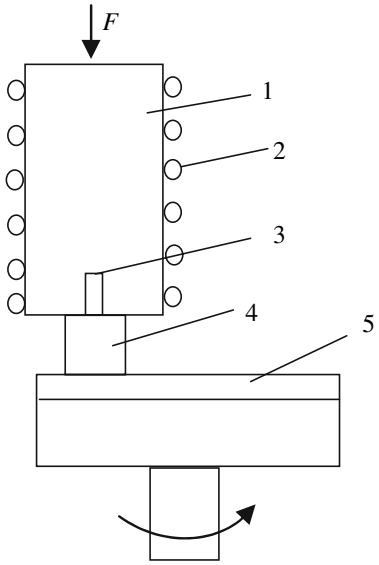

Fig. 2 Schematic diagram of wear test device: 1—Sample holding part; 2—Heating part; 3—Pin type wear sample; 4—Temperature controlling part; and 5—Counterface disc

were measured using a balance with an accuracy of 0.1 mg. The results of the wear tests were quantified as the volume loss of the specimen. The quoted volume loss (ΔV) for the test material is determined through Eq 2

$$\Delta V = \frac{m_1 - m_2}{\rho} \quad \text{(Eq 2)}$$

where, ΔV is the volume loss of the test material, mm^3; m_1 and m_2 are the initial and final mass of the test pin, mg; and ρ is the density of the test material, mg/mm^3.

2.5 Microstructure Examination

The investigation techniques used for microstructure characterization included X-ray diffraction (XRD), optical microscopy (OM), and scanning electron microscopy (SEM). The samples were etched with 5% natal for optical microscopy examination, while a mixture of 5 mL HCl, 45 mL 4% Picral, and 50 mL 5% nital was used as an etchant for SEM evaluation. The optical microscopy used was a Neophot 32. The SEM used was a CSM 950. XRD was employed to identify the phases in the specimens. XRD was carried on a MXP21VAHF diffractometer with Cu Kα radiation at 40 kV and 200 mA as an X-ray source. The sample was scanned in the 2θ range of 20°-90° in a step-scan mode (0.02° per step).

3. Results and Discussion

3.1 As-Cast Structure of High-Carbon HSS Roll

The as-cast structures of high-carbon HSS roll are shown in Fig. 3. It consists of the carbides and the metallic matrix. The XRD spectrum of sample demonstrates that the carbides are MC, M_2C, and M_7C_3, as shown in Fig. 4. Thereinto, M_7C_3 type or M_2C type carbides are located along solidification cell boundaries, and most of the MC-type carbides are formed inside the cells. The metallic matrix is the mixture of austenite

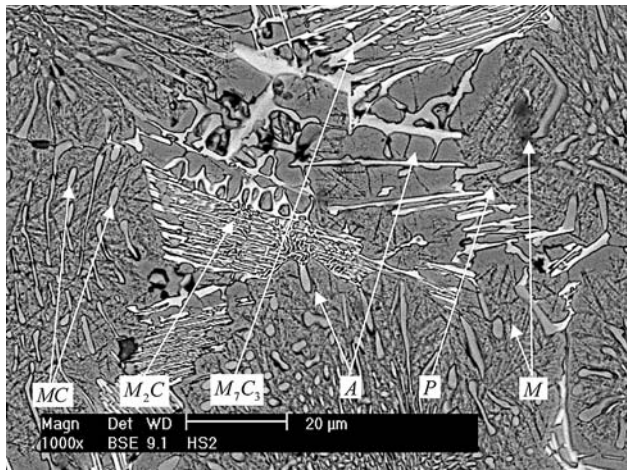

Fig. 3 As-cast microstructures of high-carbon HSS roll: *A*—Austenite; *P*— Pearlite; and *M*—Martensite

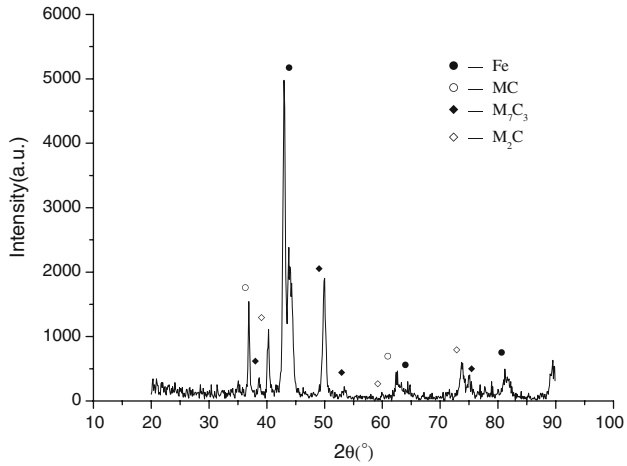

Fig. 4 XRD spectrum of cast high-carbon HSS roll

(*A*), martensite (*M*), and pearlite (*P*). The amount of austenite is the most and the amount of pearlite is the smallest.

3.2 The Role of Austenitizing Temperature on Structure

With air-cooling, a small quantity of pearlite exists in the quenching structure when the austenitizing temperature is lower than 1273 K. On the other hand, with sodium silicate solution cooling, a small quantity of pearlite exists in the quenching structure only when the austenitizing temperature is lower than 1223 K. When the austenitizing temperature reaches 1273 K, the metallic matrix transforms into the martensite, as shown in Fig. 5(a) and (b). Afterwards, the eutectic carbides dissolve into the metallic matrix and their continuous network distribution changes into the broken network with the increase of austenitizing temperature. Moreover, with the increase of austenitizing temperature, the high-temperature austenite dissolves many carbon and alloying elements, which results in the decrease of M_s point of alloy and the increase of the stability of austenite (Ref 35-37). So, the quenched structure contains some retained austenite, as shown in Fig. 5(c-f).

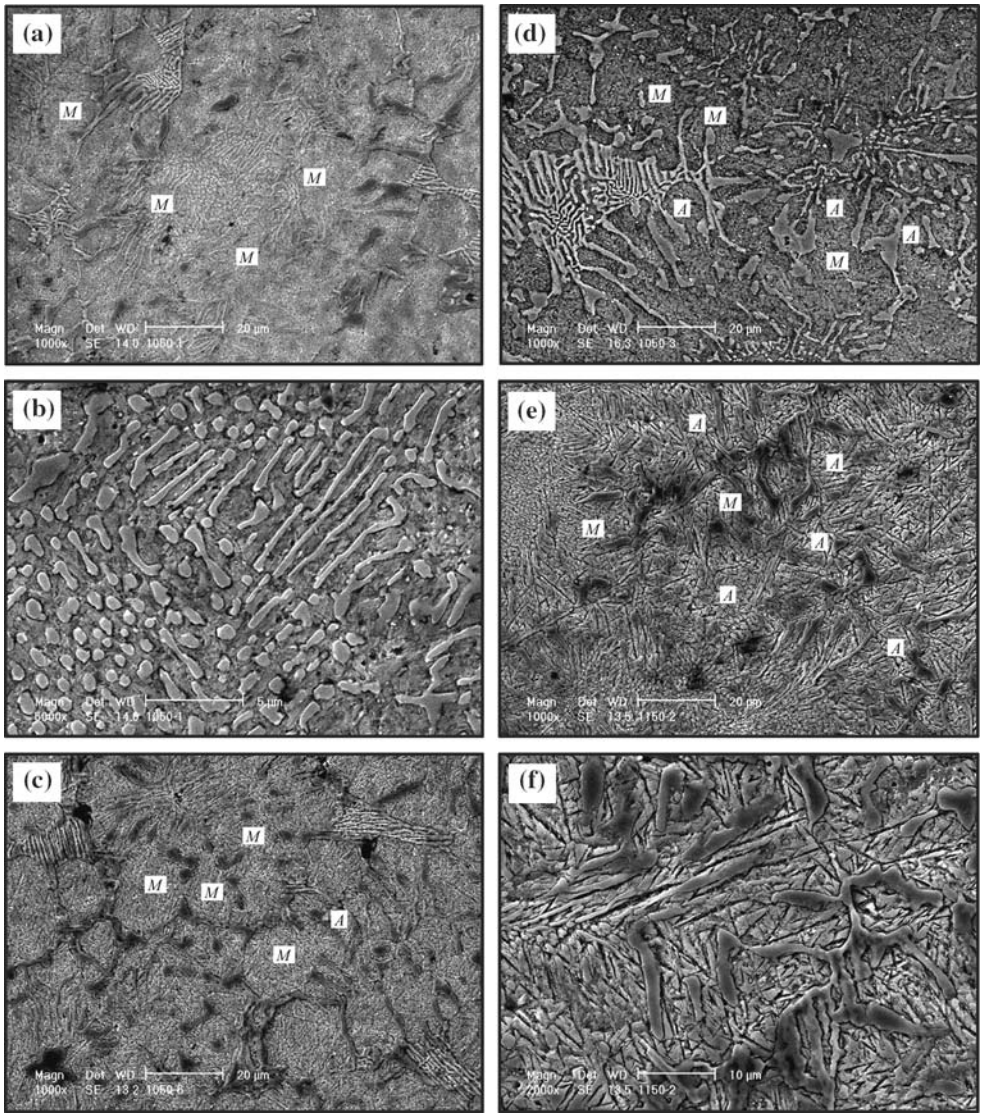

Fig. 5 Microstructures of sodium silicate solution cooling HSS roll at 1273 K (a, b), 1323 K (c), 1373 K (d), and 1423 K (e, f)

3.3 Effect of Austenitizing Temperature and Quenchant on Hardness

Figure 6 shows the effects of austenitizing temperature and quenchant on the hardness of high-carbon HSS roll. The hardness goes up until the austenitizing temperature reaches 1323 K while cooling in the sodium silicate solution and drops down as the temperature exceeds 1323 K, as shown in Fig. 6(a). The hardness obtained in air-cooling exhibits a similar tendency as that in the sodium silicate solution cooling process, as shown in Fig. 6(b). The hardness of quenched HSS roll is affected not only by the microstructure, but also by the quantities of carbon and alloy elements in the martensite and the residual austenite (Ref 38, 39). When quenched at a lower temperature, there are less carbon and alloy elements dissolved in the austenite. Saturated carbon and alloy elements in the martensite are small after quenching, resulting in lower hardness of the material. When heating temperature is below 1273 K, the microstructure would transform to pearlite with lower hardness because the specimens were not heated high enough. On the contrary, when the austenitizing temperature excels 1373 K, there would be too much carbon and alloy elements dissolved in the austenite. The austenite would become stable with the decrease of M_s point (Ref 35-37), more residual austenite remaining in the microstructure after quenching (shown in Fig. 5e and f) would result in distinctly lower hardness of the material. Adequate carbon and alloy elements would dissolve in the austenite, which transforms to the martensite during the cooling. The highest hardness is obtained as a result of the austenitizing temperature being chosen to be around 1323 K.

Figure 7 shows the change of retained austenite in the quenching structure. The retained austenite amount increases with the increase of austenitizing temperature. Figure 8 is the XRD spectrums of sample at different austenitizing temperature. Along with the increase of austenitizing temperature, the peak values of carbides decrease and the amount of carbides dissolved into the metallic matrix increases, resulting in the increase of retained austenite in the quenching structure.

3.4 Effect of Tempering on Mechanical Property

Figure 9 shows the effects of tempering temperature on the hardness of high-carbon HSS roll. No significant change in

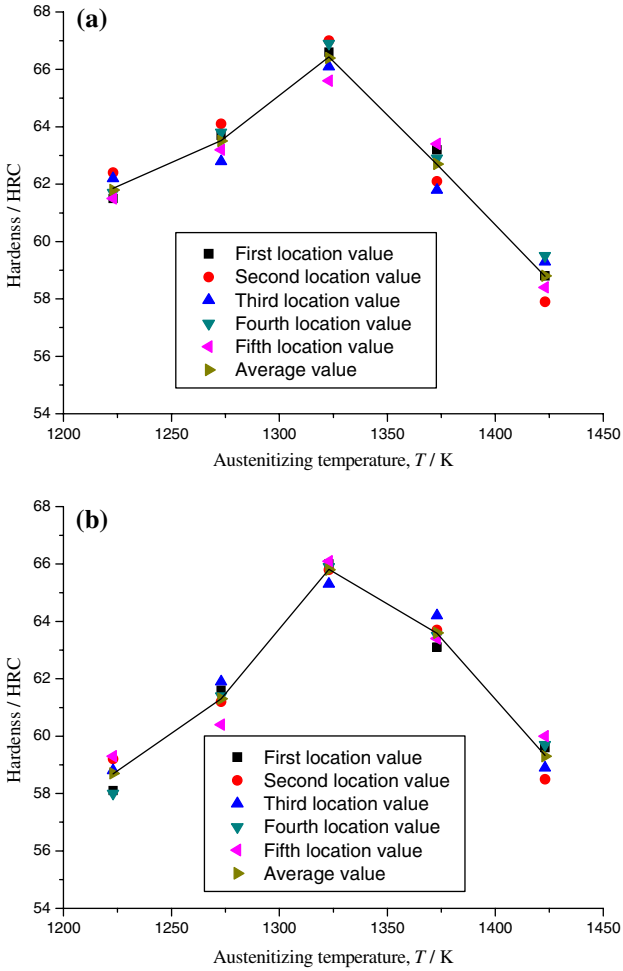

Fig. 6 Effect of austenitizing temperature and quenchant on hardness of high-carbon HSS roll: (a) sodium silicate solution cooling; and (b) air-cooling

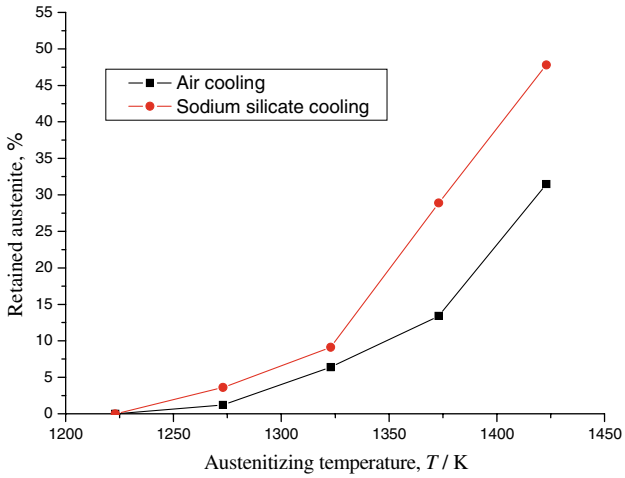

Fig. 7 Effect of austenitizing temperature and quenchant on retained austenite

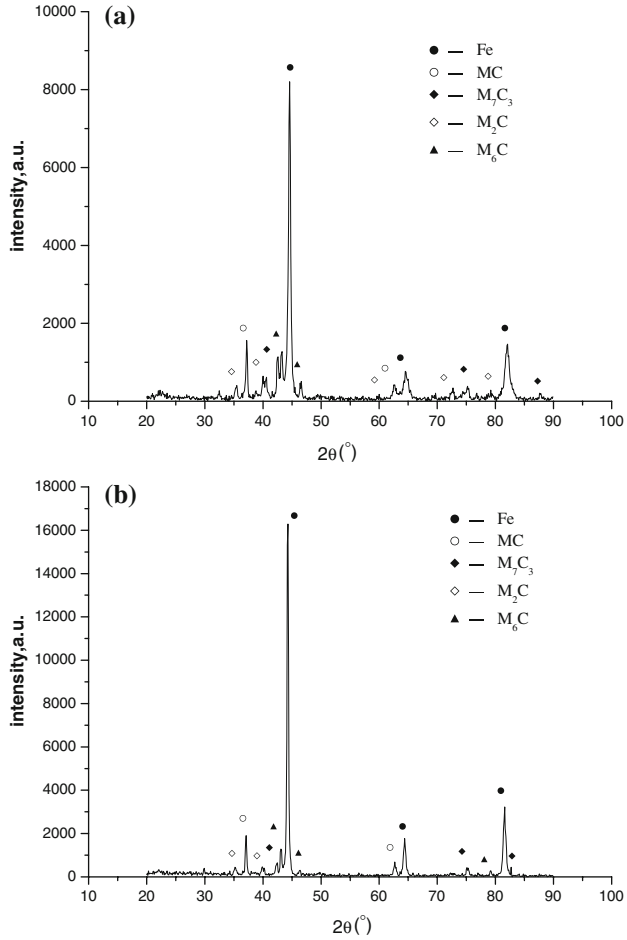

Fig. 8 XRD spectrum of samples quenching with sodium silicate cooling: (a) quenching at 1273 K; and (b) quenching at 1423 K

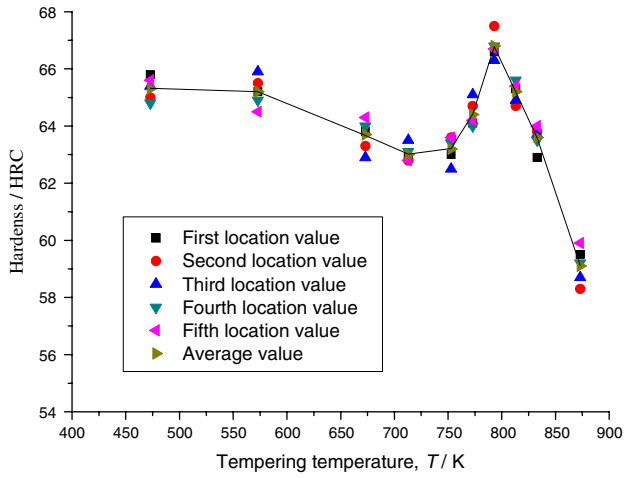

Fig. 9 Effect of tempering temperature on hardness of sodium silicate solution cooling high-carbon HSS roll at 1323 K

hardness is observed unless the tempering temperature is beyond 573 K. When the tempering temperature exceeds 573 K, the hardness decreases slightly; however, the hardness increases obviously while the tempering temperature excels 773 K and reaches a peak value around 793 K. Figure 10 shows the effects of tempering temperature on the tensile strength and elongation percentage of high-carbon HSS roll.

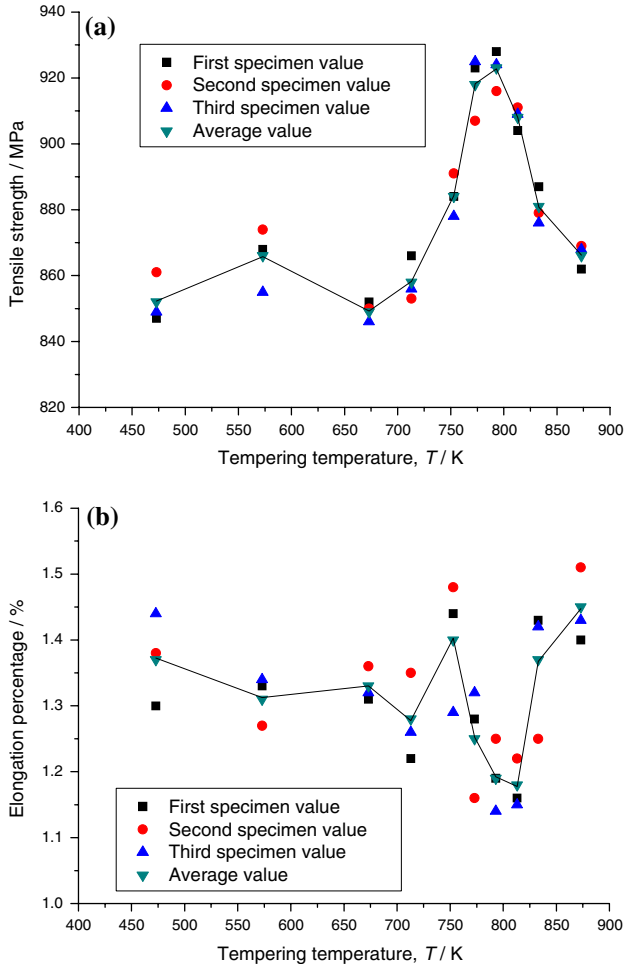

Fig. 10 Effect of tempering temperature on tensile strength (a) and elongation percentage (b) of sodium silicate solution cooling high-carbon HSS roll at 1323 K

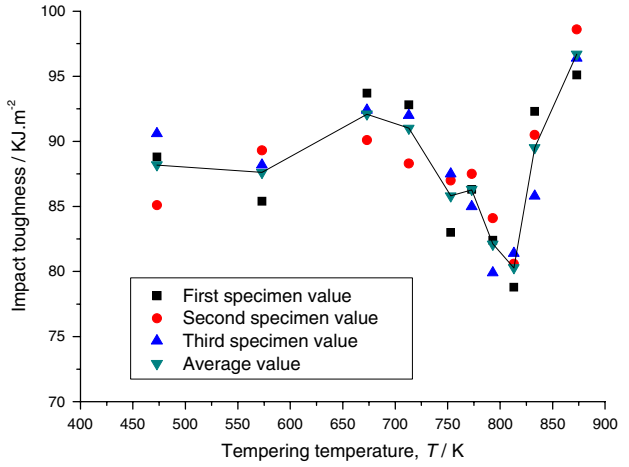

Fig. 11 Effect of tempering temperature on impact toughness of sodium silicate solution cooling high-carbon HSS roll at 1323 K

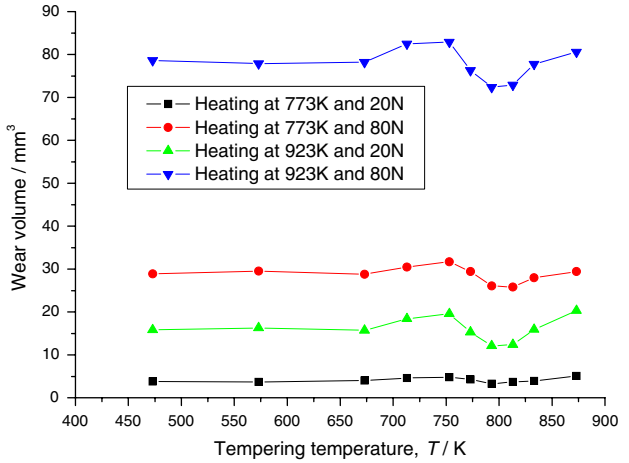

Fig. 12 Effect of tempering temperature on wear volume of sodium silicate solution cooling high-carbon HSS roll at 1323 K

Under 753 K, the tensile strength and elongation percentage of high-carbon HSS roll have no obvious change. When the tempering temperature excels 753 K, the tensile strength increases obviously, and the elongation percentage decreases slightly. When the tempering temperature exceeds 813 K, the tensile strength decreases and the elongation percentage increases. Figure 11 shows the effects of tempering temperature on the impact toughness of high-carbon HSS roll. Under 773 K, the impact toughness of high-carbon HSS roll has no obvious change. When the tempering temperature excels 773 K, the impact toughness has a slight decrease. When the tempering temperature exceeds 833 K, the impact toughness begins to increase.

No significant changes in hardness and tensile strength are observed unless the tempering temperature is beyond 573 K, because the carbide amount precipitating in the martensite is small and the austenite cannot decompose (Ref 37, 40). Tempering at 673-773 K, the supersaturated carbon separates out and the carbon concentration in the martensitic matrix decreases. These factors result in the decrease of hardness and tensile strength. Tempering at 793 K, the martensite changes into the tempered martensite containing many fine alloy carbides, and the martensitic transformation of the residual austenite accomplishes in the cooling (Ref 19, 37), leading to hardening and strengthening of HSS roll. When the tempering temperature increases further, alloy carbides begin to grow and coarsen, leading to the decrease of hardness.

3.5 Effect of Tempering Temperature on Abrasion Resistance

The effects of tempering temperature on the abrasion resistance (namely wear volume) of high-carbon HSS roll are shown in Fig. 12. In the same load and heating temperature, high-carbon HSS roll tempering at 473-673 K has smaller wear volume and excellent abrasion resistance. The abrasion resistance begins to decrease beyond the above temperature. However, the abrasion resistance presents a rising tendency beyond 773 K and begins to decrease beyond 813 K. Moreover, the wear amount of HSS roll at a higher load (80 N) is larger than that at a lower load (20 N). In the same tempering temperature and test load, the wear amount of HSS roll heating at 773 K is lower than that at 923 K. Because there are many vanadium, molybdenum, niobium, cobalt, and chromium, etc.,

alloy elements in high-carbon HSS roll, and the red hardness of HSS roll is high. When the heating temperature reaches 873 K, the hardness of HSS roll still keeps above 60 HRC (Ref 41, 42). When the heating temperature is beyond 873 K, the hardness descends obviously (Ref 41, 42). So the wear amount of HSS roll is minor heating below 873 K and increases rapidly heating beyond 873 K.

3.6 Application of Heat-Treatment Process in the Production of HSS Roll

The above heat-treatment process has been used in the production of high-carbon HSS roll. The shape and dimension of finished HSS rolls are shown in Fig. 1. Thereinto, the outer diameter of roll is Ø330 mm, the inner diameter of roll is Ø220 mm, and the height of roll is 90 mm. The austenitizing temperature is 1320-1330 K. The holding time is 150-180 min, sodium silicate solution cooling. The tempering temperature is 790-800 K. The holding time is 380-400 min, air-cooling. The hardness of HSS roll is 64-66 HRC, the range of hardness variation in the roll surface is smaller than 2 HRC. The steel pipe output of HSS rolls is about 25,000-28,000 tons, and the steel pipe output of PM hard alloy rolls is 29,600 tons, and the steel pipe output of high-chromium white cast iron rolls is only 2750 tons used in the tensile reducing diameter mills of steel pipe. The service life of HSS rolls is eight times longer than that of high-chromium white cast iron rolls and the service life of HSS rolls and PM hard alloy rolls is equivalent, and there are no crack and spalling in the use. Furthermore, the manufacturing costs of HSS rolls, PM hard alloy rolls, and high-chromium white cast iron rolls are 150, 500, and 50 yuan per kg, respectively. The manufacturing cost of HSS rolls is obviously lower than that of PM hard alloy rolls, which is only 30% of that of PM hard alloy rolls.

4. Conclusion

Based on the above results, the following conclusions can be drawn:

(1) With air-cooling and sodium silicate solution cooling, when the austenitizing temperature reaches 1273 K, the metallic matrix transforms into the martensite. Afterwards, the eutectic carbides dissolve into the metallic matrix and its continuous network distribution changes into the broken network.
(2) With the increase of austenitizing temperature, the hardness of high-carbon HSS roll increases. When the austenitizing temperature excels 1323 K, the hardness decreases.
(3) No significant change in hardness is observed unless the tempering temperature is beyond 573 K. The hardness increases obviously while the tempering temperature excels 773 K, and reaches a peak value around 793 K.
(4) No significant changes in tensile strength and elongation percentage are observed unless the tempering temperature is beyond 753 K. The tensile strength increases obviously and the elongation percentage decreases slightly beyond 753 K. When the tempering temperature exceeds 773 K, the impact toughness has a slight decrease and begins to increase beyond 833 K.
(5) The abrasion resistance begins to decrease beyond 673 K and presents a rising tendency beyond 773 K. When tempering temperature exceeds 813 K, the abrasion resistance begins to decrease. Tempering at 793-813 K, high-carbon HSS roll presents smaller wear volume and excellent abrasion resistance.
(6) The service life of high-carbon HSS rolls austenitizing at 1320-1330 K for 150-180 min and tempering at 790-800 K for 380-400 min is eight times longer than that of high-chromium white cast iron rolls used in the tensile reducing diameter mills of steel pipe.

Acknowledgments

The authors would like to thank the financial support for this work from the innovation fund of small and medium-sized enterprise of Science & Technology Ministry of China under grant (07C26215110842).

References

1. L. Sun, Q. Zhang, X. Chen, B. Wu, Z. Yu, and L. Li, Application of Simulated Annealing Algorithm to Improve Work Roll Wear Model in Plate Mill, *J. Univ. Sci. Technol. Beijing*, 2002, **9**, p 224–227
2. H. Furumoto, K. Yamada, and J. Yanagimoto, Effect of the Number of Work-Roll Surface Division on Prediction of Contact Length in Coupled Analysis of Roll and Strip Deformation During Sheet Rolling, *ISIJ Int.*, 2002, **42**, p 736–743
3. R.R. Xavier, M.A. De Carvalho, E. Cannizza, T.H. White, A. Rivaroli Jr., and A. Sinatora, High-Speed Steel Rolls for Long Products, *Iron Steel Technol.*, 2004, **1**, p 28–33
4. K. Ichino, S. Ishikawa, Y. Kataoka, and T. Toyooka, Improvement of Hot Wear Characteristic of High Speed Tool Steel Roll by Increase in Cr and Mo Contents, *J. Iron Steel Inst. Jpn.*, 2003, **89**, p 680–685
5. M. Andersson, R. Finnstrom, and T. Nylen, Introduction of Enhanced Indefinite Chill and High Speed Steel Rolls in European Hot Strip Mills, *Ironmak. Steelmak.*, 2004, **31**, p 383–388
6. C.K. Kim, J.I. Par, S. Lee, K.Y. Chan, N.J. Kim, and Y.J. Seung, Effects of Alloying Elements on Microstructure, Hardness, and Fracture Toughness of Centrifugally Cast High-Speed Steel Rolls, *Metall. Mater. Trans. A*, 2005, **36**, p 87–97
7. K. Ichino, Y. Kataoka, and T. Koseki, Development of Centrifugal Cast Roll with High Wear Resistance for Finishing Stands of Hot Strip Mill, *Kawasaki Steel Tech. Rep.*, 1997, **37**, p 13–18
8. K. Gong, Y. Dong, and C. Gao, Research and Manufacture of Compound High Speed Steel Rolls, *Iron Steel (Peking)*, 1998, **33**, p 67–71
9. M. Shimizu, O. Shitamura, S. Matsuo, T. Kamata, and Y. Kondo, Development of High Performance New Composite Roll, *ISIJ Int.*, 1992, **32**, p 1244–1249
10. M. Hashimoto, S. Otomo, and K. Yoshida, Development of High-Performance Roll by Continuous Pouring Process for Cladding, *ISIJ Int.*, 1992, **32**, p 1202–1210
11. T. Tanaka, H. Takigawa, and M. Hashimoto, The Application and Performance of High-Speed-Steel (HSS) Rolls at Hot Rolling, *Mechanical Working and Steel Processing Conference Proceedings* (Warrendale, PA), The Iron and Steel Society, Inc., 1998, **35**, p 435–444
12. Y. Ikawa, T. Itami, K. Kumagai, Y. Kawashima, A.G. Leatham, J.S. Coombs, and R.G. Brooks, Spray Deposition Method and Its Application to the Production of Mill Rolls, *ISIJ Int.*, 1990, **30**, p 756–763
13. C.D. Zhou, J.F. Fan, H.R. Le, Y.J. Lin, D.S. Sun, and J.G. Zhang, Microstructural Characteristics and Mechanical Properties of Spray Formed High Speed Steel for Work Roll, *Acta Metall. Sin. (English Lett.)*, 2004, **17**, p 548–553

14. H. Fu, A. Zhao, and J. Xing, Development of Centrifugal Casting High Speed Steel Rolls, *J. Univ. Sci. Technol. Beijing*, 2003, **10**, p 61–66
15. K. Ichino, Development of Centrifugal Cast HSS Roll with Excellent Surface Deterioration Resistance in Hot Strip Mill, *CAMP-ISIJ*, 2002, **15**, p 995
16. Z. Xin and M.C. Perks, Centrifugal Casting of HSS Roll for Narrow Strip and Rod Mills, *42nd Mechanical Working and Steel Processing Conference Proceedings* (Warrendale, PA), The Iron and Steel Society, Inc., 2000, **38**, p 183–191
17. L. Xu, J. Xing, S. Wei, H. Chen, and R. Long, Comparative Investigation to Rolling Wear Properties Between High-Vanadium High-Speed Steel and High-Chromium Cast Iron, *J. Xi'an Jiaotong Univ.*, 2006, **40**, p 275–278
18. S. Wei, J. Zhu, and L. Xu, Effects of Vanadium and Carbon on Microstructures and Abrasive Wear Resistance of high Speed Steel, *Tribol. Int.*, 2006, **39**, p 641–648
19. H. Zhou, J. Wang, Y. Su, J. Lian, and K. Ogi, Heat Treatment of High Carbon Vanadium High Speed Steel for Roller, *Iron Steel (Peking)*, 2000, **35**, p 47–50
20. Y. Zhao, Y. Cai, and R. Xu, Composition Design and Heat Treatment of High-Speed-Steel Rolls, *J. Liaoning Tech. Univ. (Natural Science Edition)*, 2003, **22**, p 836–838
21. Yu M. Kuskov, High-Alloy High-Speed Steels for Rollers, *Stal'*, 2004, **4**, p 43–48
22. J. Tuo, S. Chen, Z. Li, C. Liu, and H. Li, Effect of Laser Surface Modification on Microstructure and Hardness of High Speed Steel Roll, *Heat Treat. Metals*, 2006, **31**, p 56–59
23. ASTM E-8, *Annual Book of ASTM Standards*, 03.01, p 545–557
24. C.P. Tabret and I.R. Sare, Effect of Heat Treatment on the Abrasion Resistance of Alloy White Irons, *Wear*, 1997, **203-204**, p 206–219
25. C.P. Tabrett and I.R. Sare, Effect of High Temperature and Sub-Ambient Treatments on the Matrix Structure and Abrasion Resistance of a High-Chromium White Iron, *Scripta Mater.*, 1998, **38**, p 1747–1753
26. L.E. Zevin and G. Kimmel, *Quantitative X-ray Diffractometry*. Springer, New York, 1995
27. C.M. Kim, X-Ray Method of Measuring Retained Austenite in Heat Treated White Cast Irons, *J. Heat Treat.*, 1979, **1**, p 43–51
28. X. Fan, *Metallography of X-Ray*. Machinery Industry Press, Beijing, 1981
29. W. Bai, S. Wei, R. Long, L. Xu, Z. Dong, and X. Yang, Effects of Retained Austenite on Rolling Wear Properties of High Vanadium High Speed Steel, *Lubr. Eng.*, 2007, **32**, p 66–72 (in Chinese)
30. Measurement of Retained Austenite in the Steel – X-ray Diffractometer Method. GB8362-1987
31. H. Fu and Z. Jiang, A Study of Abrasion Resistant Cast Fe-B-C Alloy, *Acta Metall. Sin.*, 2006, **42**, p 545–548
32. H. Shi, H. Fu, and W. Zhang, A Study on Low-Alloy Cast Steel Wear-Resistance Hammer with Multi-Phase, *Foundry*, 2001, **51**, p 103–105 (in Chinese)
33. Z. Liu, Friction and Wear Characteristics of M50 High Speed Steel at Elevated Temperature, *Tribology*, 1997, **17**, p 38–44 (in Chinese)
34. H. Fu, J. Liu, and J. Xing, Study on Microstructure and Properties of High Speed Steel Guide Plate Modified by RE-Mg-Ti, *J. Iron Steel Res.*, 2003, **15**, p 39–43 (in Chinese)
35. K.C. Hwang, S.H. Lee, and H.C. Lee, Effects of Alloying Elements on Microstructure and Fracture Properties of Cast High Speed Steel Rolls Part I: Microstructural Analysis, *Mater. Sci. Eng.*, 1998, **A254**, p 282–295
36. K. Yamamoto, T. Kogin, T. Harakawa, N. Murai, M. Kuwano, and K. Ogi, Effects of Alloying Elements in Hardenability for high C High Speed Steel Type Alloy, *Imono*, 2000, **72**, p 90–95
37. Y. Deng, J. Chen, and S. Wang, *High Speed Tool Steel*. Metallurgical Industry Press, Beijing, 2002
38. C. Ernst, E. Haberling, and K. Rasche, Carbide Dissolution and Precipitation Processes During Hardening of a High-Speed Steel, *Stahl und Eisen*, 1995, **115**, p 71–76
39. R.A. Nogueira, O.C.S. Ribeiro, M.D.M. Das Neves, L.F.C.P. De Lima, F.A. Filho, D. Friedrich, and L. Boehs, Influence of the Heat Treatment on the Microstructure of AISI T15 High Speed Steel, *Mater. Sci. Forum*, 2003, **416-418**, p 89–94
40. L.A. Dobrzanski and W. Kasprzak, Influence of 5% Cobalt Addition on Structure and Working Properties of the 9-2-2-5, 11-2-2-5 and 11-0-2-5 High-Speed Steels, *J. Mater. Process. Technol.*, 2001, **109**, p 52–64
41. Z. Qi, Q. Feng, L. Wu, and Z. Xie, Red Hardness of High Speed Steel, *Heat Treat. Metals*, 2001, **26**, p 8–11 (in Chinese)
42. N. Singh and S.R. Prabhakar, Performance Appraisal of High Speed Steel Turning Tools, *Mater. Technol.*, 2003, **18**, p 218–224